Plasmonics (2013) 8:1079–1086
DOI 10.1007/s11468-013-9512-3

Dipole Decay Rates Engineering via Silver Nanocones

Stefania D'Agostino · Fabio Della Sala · Lucio Claudio Andreani

Received: 6 October 2012 / Accepted: 30 January 2013 / Published online: 1 March 2013

Abstract A full control of the interaction between confined plasmons and point sources of radiation is a central issue in molecular plasmonics. In this paper, a theoretical contribution towards a physical understanding on the localized surface plasmons excited into metallic nanocones by a point dipole is given. A numerical approach based on the discrete dipole approximation is applied to determine the modifications of the dipole decay rates for varying geometrical parameters of the dipole-metal nanoparticle system. Results declare the centrality of the cone aperture to control the plasmon resonances and to handle the effects it induces on the lifetime of a point emitter. A full spectral tuning of the resonances in the decay rates can be achieved by operating on a unique spatial degree of freedom: by tailoring the aperture alone, total decay rates 10^5 times higher than the free-space value can be obtained at short distances from the metal in a large region of the spectral range. Quite unexpectedly, size dependence of the antenna is found to have a marginal role if only a lifetime manipulation is desired. It becomes, instead, a crucial aspect of the problem when large quantum yields are required. Results presented in this work shed light on spontaneous emission modification due to interaction with plasmonic nanocones of different shapes and are relevant for a number of applications in the fields of nanoplasmonics and fluorescence microscopy.

Keywords Plasmonics · Decay rates · Dipole

S. D'Agostino (✉) · L. C. Andreani
Dipartimento di Fisica, Università degli Studi di Pavia,
Via Bassi, 6, 27100 Pavia, Italy
e-mail: stefania.dagostino@unipv.it

F. Della Sala
National Nanotechnology Laboratory (NNL),
Istituto Nanoscienze-CNR,
Via per Arnesano 16, 73100 Lecce, Italy

F. Della Sala
Center for Biomolecular Nanotechnologies @UNILE,
Istituto Italiano di Tecnologia,
Via Barsanti, 73010 Arnesano, Italy

Introduction

In the last years, the radiative decay rate engineering has become a central issue in nanophotonics. The development of nano-optic techniques has affirmed the importance of exploiting plasmonic nanoantennas [1], like metallic nanostructures, nanoparticles (NPs), or NP aggregates, to achieve the engineering of the decay rates and, thus, to modify the excited-state lifetime [2], the fluorescence intensity [3–6], and the radiation pattern [7, 8] of isolated emitters [9–11].

Among optical antennas a particular attention has been paid in the last years to plasmonic objects able to effectively replace conventional focusing lenses, by confining radiation to dimensions much smaller than the diffraction limit (superfocusing phenomenon) [12–14], such as nanorods, tapered or V-shaped nanostructures, tips, cones, and bow-tie or bridged antennas [15–20]. For these objects, the strong local fields, due also to the lightning rod effect produced by the sharp edges and curvatures, make both the phenomena of metal-enhanced fluorescence and lifetime reduction to be observed also at the same time [21]. From confocal fluorescence imaging of Chinese hamster ovary cells grown on a randomly distributed Ag-coated silicon nanocones, as an example, a reduction in the lifetime of R6G has been detected together with an amplification of the fluorescence intensity up to 100-fold the value registered on glass substrates [21]. Beyond fluorescence spectroscopy, due to the

high field localization and enhancement they can achieve, conically shaped nanoparticles have found also widespread applications in optical imaging techniques with nanometer spatial resolution, such as tip-enhanced or scattering-type near-field microscopy [22], atomic force microscopy [12], scanning probe microscopy [23], and light emission in scanning tunneling microscopy [24], as well as in surface-enhanced spectroscopies such as Raman scattering [12], tip-enhanced Raman scattering [25], infrared absorption [26], and coherent nonlinear optics such as second-harmonic generation [27]. Combining optical spectroscopy with scanning probe methods, conically shaped nanoparticles uniquely allow for optical spectroscopy with ultrahigh spatial resolution down to 10 nm. Moreover, an advantage of such tip structures is that they offer field enhancement along the third dimension, away from the planar surface, which could be useful for certain lab-on-a-chip applications useful for analyte detection or biological studies, such as spectroscopy of cells [28] and optical trapping applications for example [21]. State-of-the-art methods for constructing nanocone structures seem to be fast, robust, and reproducible so that high-quality sharp tips with apex radii of a few nanometers can be obtained [12, 29–32]. All of the above applications concur in making nanocones very promising objects for molecular plasmonics studies.

From a theoretical point of view, the investigation of electrodynamic coupling between molecules and metal nanoparticles can be treated with different levels of approximations, and different options can be found in the literature [9, 33–46]. Concerning conically shaped nanoparticles, Thomas et al. [39] compute the radiative and the nonradiative decay rates for silver tips of parabolic shape with a numerical approach based on a surface-integral formalism. The work shows the importance of perpendicular orientation of the dipole in ensuring a high quantum yield and how the presence of defect strongly modifies the spectral behavior of the decay [39]. More recently, Mogammadi et al. [46] calculate the Purcell factors and the antenna efficiencies for single and double truncated Au nanocones by using the finite difference time domain method. The numerical study illustrates a great advantage of nanocones (compared to nanorods and nanospheroids), since the spectral position of the localized surface plasmons (LSPs) can be tuned toward shorter wavelengths without compromising the Purcell factor or reducing the antenna efficiency [46].

In this work, we focus the attention on the electromagnetic interaction between Ag nanocones of different apertures and sizes and a point-like emitter located along their symmetry axes. The radius of curvature of the analysed tips is considered negligible ($r_c \simeq 0$). This interest is supported by the experimental trend to realize sharp cones: state-of-the-art fabrication techniques allow to reach values of the radius of curvature of tapered waveguides below 5 nm [12, 13]. The behavior of rounded tips is already known in literature [39, 46] and is not examined here.

Here, we adopt a classical electrodynamics description of the metal emitter coupling in order to study the field enhancement and the modifications of the spontaneous decay rate of the emitter. The system is assumed to be in a weak-coupling regime, and a macroscopic description of metal is assumed to be valid [47]. Numerical results reported here declare the centrality of aperture to control the plasmon resonances of a conically shaped nanoparticle and to handle the effects they induce on the lifetime of a punctual emitter. A spectral tuning of the resonances in the decay rates can be achieved by operating on a unique spatial degree of freedom: by tailoring the aperture alone, total decay rates 10^5 times higher than the free-space value can be obtained at short distances from the metal in the near-infrared (NIR) region of the spectral range. As an unexpected result, size dependence of the antenna behavior turns out to have a marginal role if only a lifetime manipulation is desired. It becomes, instead, a crucial aspect of the problem when large quantum yields are required. Results presented could be of interest for fundamental properties of light–matter interaction (possibly also in view of achieving the strong-coupling regime [48]) and for microscopies and surface-enhanced spectroscopy applications. In particular, by giving new information on the huge potentialities of cones in increasing the decay rates of a dipole in the visible and in the infrared spectral ranges, we believe that the present work could open new avenues for a wise use of such plasmonics structures in *in vitro* "optical biopsy" of tissues or other diagnostic techniques based on the analysis of fluorescence signals.

Method

In this work, the total, radiative, and nonradiative decay rates are computed by varying the spectral and spatial degrees of freedom of the system in a numerical framework based on the discrete dipole approximation (DDA) [49]. This approach is general and accurate and allows to investigate coupling problems involving complex nanoparticle shapes which cannot be easily treated with other (analytic or ab initio) methods. DDA is a numerical method which describes the metal as an array of polarizable dipolar elements (named grid points in the next sections) organized on a lattice to represent the shape of the nanoparticle and is usually applied to find the solution of Maxwell's equations for arbitrarily shaped metallic nanoparticles excited with plane waves or other far-field radiations [50].

In this paper, an extension of the method to include incident dipolar fields as incident radiation is used. This extension is incorporated in the code of ADDA [51], whose

main feature is the ability to parallelize a single DDA simulation by running on a multiprocessor system. If we assume a point-like dipole $\tilde{\mathbf{p}}_0$ located at $\mathbf{r}_0$ and oscillating with frequency ω_{exc} emitting electromagnetic radiation, the metallic nanoparticle will reflect and/or scatter back the radiation by generating an electric field $\widetilde{\mathbf{E}}_{\text{scat}}$ at the dipole position. This will produce a change in the decay dynamics of the emitter given by [52]

$$\frac{\Gamma}{\Gamma_0} = 1 + \frac{6\pi\varepsilon_0\tilde{\varepsilon}_B q_0}{k^3\left|\tilde{\mathbf{p}}_0\right|^2} Im\left[\widetilde{\mathbf{p}}_0^* \cdot \widetilde{\mathbf{E}}_{\text{scat}}\left(\mathbf{r}_0\right)\right], \tag{1}$$

where q_0 is the intrinsic quantum yield of the dipole, $\tilde{\varepsilon}_B$ is the relative dielectric constant of the background medium, and Γ_0 is the decay rate in free space, corresponding to the total radiated power of a molecule in free space normalized to the energy of the emitted photons, if no internal losses are present.

The idea underlying the approach used in this work is, thus, to describe the local field in the dipole position by recurring to the numerical solution of the Maxwell problem obtainable with DDA. By solving in a self-consistent way, a system of $3N$ coupled complex equations, DDA gives the N polarizabilities $\tilde{\mathbf{p}}_i$ describing the polarization status of the target, so that the *normalized absorption efficiency* (NAE), the scattered field experienced by the dipole, as well as its total, radiative, and nonradiative decay rates can be calculated. For normalized absorption efficiency, we intend the DDA absorption efficiency normalized on the squared modulus of the dipole (NAE $= Q_{\text{abs}}/\left|\tilde{\mathbf{p}}_0\right|^2$), this being mandatory to obtain spectra independent from the source. The DDA efficiency Q_{abs} is calculated, as usual, by dividing the absorption cross section over the area of the geometrical cross section of the sphere with volume equal to that of the dipole representation of the particle (πa_{eff}^2). Unless otherwise specified, the Palik dielectric function [53] and an interdipole distance of $d_{\text{int}} = 0.0625 = 1/16$ nm are used in describing the metallic nanostructures.

Results

The results here presented are obtained by exciting an Ag nanocone only by a dipolar field generated by a point-like source (like a fluorophore or a quantum dot) put in its proximity; external plane wave radiations are assumed to be absent. A complex dipole is assumed to oscillate along the symmetry axis of Ag cone: this kind of orientation being preferred [39]. The analysis has been performed by considering the response of the metallic cone as a function of its geometrical parameters (aperture and size) as well as of the dipole excitation wavelength (λ_{exc}).

Role of Aperture

Firstly, we consider Ag cones with a fixed height (20 nm) and different base radii: 3, 5, 11, 20, and 35 nm. We will refer to the different cones with their aperture or tip angle, given by $\approx \pi/21$, $\pi/13$, $\pi/6$, $\pi/4$, and $\pi/3$ radians, respectively. A schematization of the system is visualized in Fig. 1.

The aim of such kind of study is to shed light on the effects of aperture either on the NAE or on the decay dynamics of an Ag cone. As a first step, we analyze the frequency dependence of the NAE for the different apertures. To do this, we fix the distance of the dipole from the cone tip to $d = 2$ nm and change the oscillation frequency in the VIS-NIR spectra range ($\lambda_{\text{exc}} \in [300 : 1200]$ nm). In Fig. 2, the NAE spectra are reported for the five apertures by considering either the bulk dielectric function [53] or the surface damping corrected dielectric function [54]. In considering the Palik dielectric function, we corrected the discontinuity at around 1 eV to avoid spurious peaks to appear in the spectra. As it can be observed in the figure, each system is characterized by a single resonance which can be related to the excitation of only the lower-order surface plasmons inside the nanocones. Incident light drives the conducting electrons in the metal in phase, generating collective oscillations and producing in this way a charge distribution resembling that of an electric dipole along z. Concerning the positions of the resonant frequencies with increasing cone aperture, a clear blue shift is evident in Fig. 2: the NAE peaks at 1,220 nm ($\pi/21$), 770 nm ($\pi/13$), 490 nm ($\pi/6$), 400 nm ($\pi/4$), and 360 nm ($\pi/3$).

Moreover, like well visible in Fig. 2, the curves obtained for the two descriptions of the metallic dielectric function are similar (except that for an intensity difference

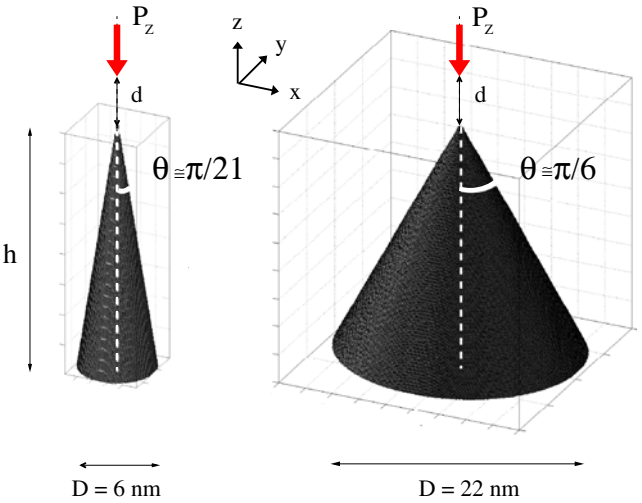

Fig. 1 Schematization of two of the analyzed systems ($\theta \approx \pi/21$ rad and $\theta \approx \pi/6$ rad, with the fixed height h =20 nm)

which increases at decreasing aperture), and no shifts in frequency can be observed. For this reason, to avoid including size-dependent approximations (which are still not well established) into the model, in our following analysis, we consider only the bulk dielectric function.

As a second step, we analyze the frequency dependence of the normalized total, radiative, and nonradiative decay rates for the different apertures. In the two panels of Fig. 3, the normalized radiative (a) and total (b) decay rates for the five analyzed Ag cones are reported. Once again, distinct resonant peaks can be observed in the spectra, with a blue shift at increasing cone aperture. The total decay rate peaks at 1,220 nm ($\pi/21$), 770 nm ($\pi/13$), 490 nm ($\pi/6$), 410 nm ($\pi/4$), and 370 nm ($\pi/3$), and for the two largest analyzed apertures ($\pi/4$ and $\pi/3$), the peaks in the total decay rate have a weak blue shift (10 nm) with respect to the radiative ones. The presence of isolated, well-defined peaks in the radiative decay rate spectra is consistent with the hypothesis that the plasmons excited inside the nanocones have dipolar character: for $l = 1$ modes, in fact, significant radiative contributions to the plasmons decay can be achieved.

We look now at the values of the normalized total decay rates in Fig. 3b. Conically shaped nanoparticles induce a huge perturbation of the total decay rate of a dipole with respect to its free-space value (up to 10^5 orders of magnitude). This means that the application of metallic nanocones in molecular plasmonics can drastically reduce the lifetime of the emitters, leading to femtosecond lifetime dynamics, the effect being more important for smaller cone apertures.

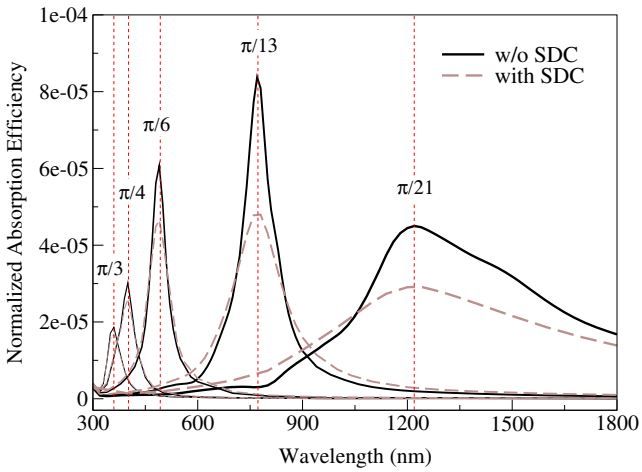

Fig. 2 Normalized absorption efficiencies for five different aperture cones ($\pi/21$, $\pi/13$, $\pi/6$, $\pi/4$, and $\pi/3$) excited with a perpendicularly oriented dipole put at 2 nm from the tip of the cone. The *solid black lines* refer to the DDA values obtained by using an Ag bulk dielectric function (without surface damping correction, SDC), while the *brown dashed lines* represent the values calculated by taking into account the correction to the bulk dielectric function due to the small size (with SDC). The used discretization parameters are $d_{\text{int}} = 1/16$ nm (for $\pi/21$, $\pi/13$, $\pi/6$, and $\pi/4$) and $d_{\text{int}} = 1/8$ nm (for $\pi/3$)

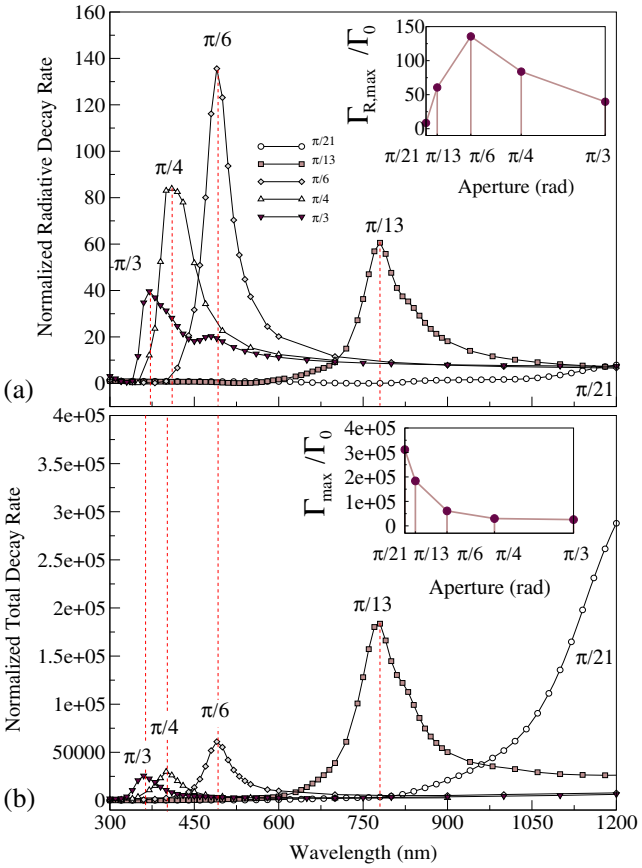

Fig. 3 Normalized radiative (**a**) and total (**b**) decay rates obtained for five different apertures ($\pi/21$, $\pi/13$, $\pi/6$, $\pi/4$, and $\pi/3$) excited with a perpendicularly oriented dipole put at 2 nm from the tip of the cone. All the decay rates are normalized to the free-space total decay rate of the dipole (Γ_0). In this scale, the nonradiative decay rates result not distinguishable from the total ones. The maxima of the radiative and total decay rates, corresponding to the peak values, respectively, in **a** and **b** are also reported and directly compared in the two insets. For what concerns $\pi/21$, the resonance is hidden by the k^3 dependence of the normalization constant Γ_0 which produces a monotonically increasing trend in the resonant region (1,220 nm). The used discretization parameters are $d_{\text{int}} = 1/16$ nm (for $\pi/21$, $\pi/13$, $\pi/6$, and $\pi/4$) and $d_{\text{int}} = 1/8$ nm (for $\pi/3$)

The major contribution to the enhancement of the total decay rate has to be ascribed to the nonradiative decay rate due to the absorption inside the metal. Radiative decay rates are increased as well (Fig. 3a), but their values are much smaller than the nonradiative ones. Concerning the trend of the enhancement by changing the angle of the cone, we should point out the monotonic decrease of the total decay rate enhancement at increasing aperture (inset in Fig. 3b), compared to the nonmonotonic behavior of the radiative decay rate (inset in Fig. 3a).

To shed light on the origin of the observed behavior, we perform an analysis of the polarization configurations on the computational grid points and of the associated internal field distribution. We consider the five cones excited at the peak

wavelengths of the total decay rate. The two-dimensional maps for the real polarizations $\mathbf{p}_i = (p_y, p_z)$ and the scattered field intensities $|\tilde{\mathbf{E}}_{\text{scat}}|^2$, normalized to $\tilde{\mathbf{p}}_0^2$, in a plane containing the dipole and perpendicular to the base are reported in Fig. 4. Globally, we can affirm that localized

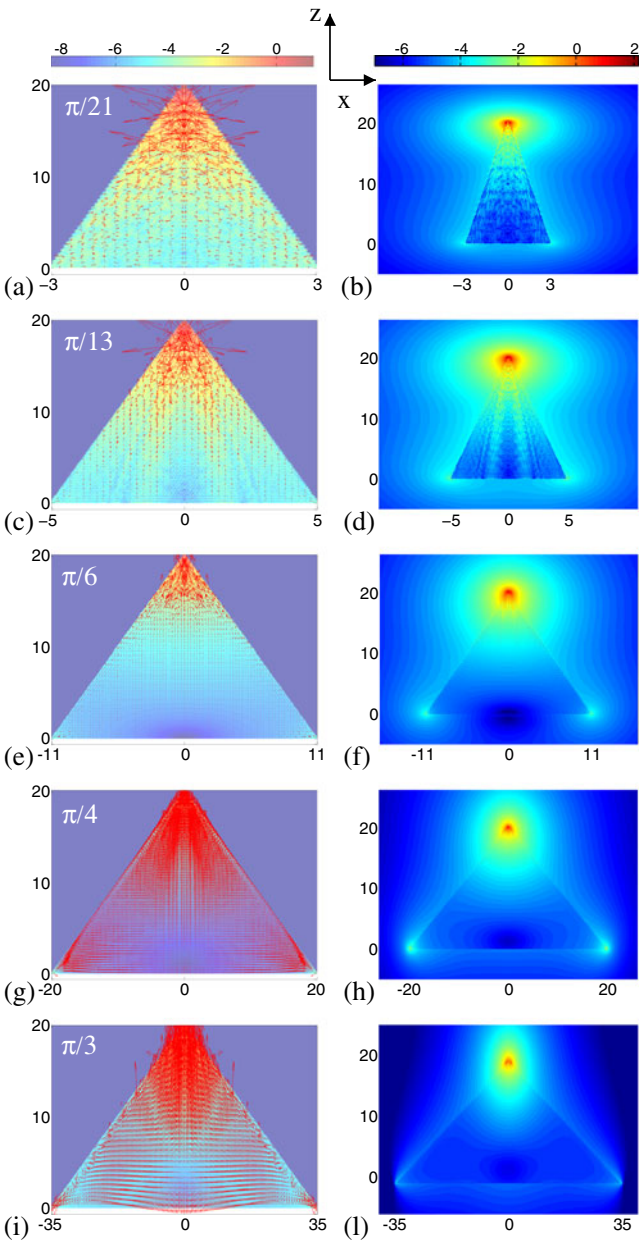

Fig. 4 *Left panels*: Polarizations (real vectors) and polarization modules, normalized to $\tilde{\mathbf{p}}_0^2$, in color scale. *Right panels*: Internal and external field modules ($\left|\tilde{\mathbf{E}}_{\text{int}}\right|^2$ and $\left|\tilde{\mathbf{E}}_{\text{scat}}\right|^2$), normalized to $\left|\tilde{\mathbf{p}}_0\right|^2$, obtained by exciting the five different cones in Fig. 3 with a dipole oscillating along the z axis at $\lambda_{\text{exc}} = 1,220$ nm ($\pi/21$), $\lambda_{\text{exc}} = 770$ nm ($\pi/13$), $\lambda_{\text{exc}} = 490$ nm ($\pi/6$), $\lambda_{\text{exc}} = 400$ nm ($\pi/4$), and $\lambda_{\text{exc}} = 360$ nm ($\pi/3$), respectively. The reported sections concern the plane xz, the coordinates are in nanometers, and the values in the color maps are in a decimal logarithmic scale. For graphical readability, the x-axis of each panel is rescaled

resonances excited inside these cones have a form which resembles a dipolar charge distribution. Anyway, as it is well visible in Fig. 4, some distinctions among resonances have to be made: the dynamically induced charge density distributions can be of diverse complexity. Panels on the left in Fig. 4 are related to the nonmonotonic behavior of the maxima in the radiative decay rate curves in Fig. 3a, while panels on the right are indicative of the internal fields and thus of the nonradiative (dissipated) power of each structure. For what concerns the internal polarizations, it results evident that the cone with the largest radiative decay rate should correspond to the cone with the largest polarization. In Fig. 4, we can observe that in the first case ($\pi/21$), no well-defined charge distributions can be identified inside the metal and that the grid dipoles are isotropically oriented, probably due to the small aperture which does not allow the internal dipoles to be oriented along a particular direction. For $\pi/13$, a polarization status similar to a dipole excitation starts to appear: grid dipoles present an important component along the z axis (that of the external oscillating dipole) even if two regions of disordered dipoles, in the form of oblique stripes, can be identified in the central region of the metallic body. In the case of $\pi/6$, the dipole resonance induced in the metal becomes more manifest with grid dipoles oriented mainly along the z axis: the excited plasmon is a dipolar state along the symmetry axis, and no contaminations from other multipole resonances can be found. By increasing the angle beyond $\pi/6$, the volume of the particle becomes large enough to allow the appearance of internal electron cloud dislocations that are more complicated than the dipolar one. For $\pi/4$ and $\pi/3$, the patterns of grid dipoles are considerably different and quadrupole arrangements of charge at the opposite sides of the base combine with the main dipolar resonance along the z axis. Although not well visible in Fig. 4, on the bottom side of the cone roughly half of the polarization points up and half down, with features typical of a quadrupolar resonance. As we expected, according to the inset of Fig. 3a, the most favorable structure turns out to be the cone with a $\pi/6$ aperture: for small aperture ($\pi/21$ and $\pi/13$), the grid dipoles are not able to align, while for big ones ($\pi/4$ and $\pi/3$), they arrange themselves to cancel the global effect (i.e., the total internal polarization).

For what concerns internal fields (see panels on the right in Fig. 4), they look similar in the five different structures, being mostly concentrated around the tip. Since the field enhancement is similar in all cases, the internal fields cannot explain the decrease in the maximum intensity of the nonradiative decay rates (inset in Fig. 3b) at increasing aperture: this behavior, instead, can be traced back to the k^3 dependence in the decay rate formula (see Eq. 1). Small apertures (see the curve for $\pi/21$) have the dipolar resonances in the NIR region and thus present huge nonradiative decay rates.

We investigate the effect of the height by considering cones with the same aperture ($\pi/13$) and different heights (40, 80, 120, and 160 nm) and larger cones with the same height (160 nm) but different apertures ($\pi/21$ and $\pi/6$). The results obtained for the normalized decay rates as well as for the quantum yields are reported in Figs. 5 and 6, respectively. For such large systems we use larger interdipole distances to reduce computing time (up to $d_{\text{int}} = 1/2$ nm). We fix the emitting dipole to 10 nm from the cone tip in order to avoid spurious effects due to the discretization. As the decay rates are rapidly decreasing with the dipole-tip distance, Fig. 5 presents decay rates not directly comparable with values in Fig. 3. Nevertheless, an accurate comparison between systems of different size is possible.

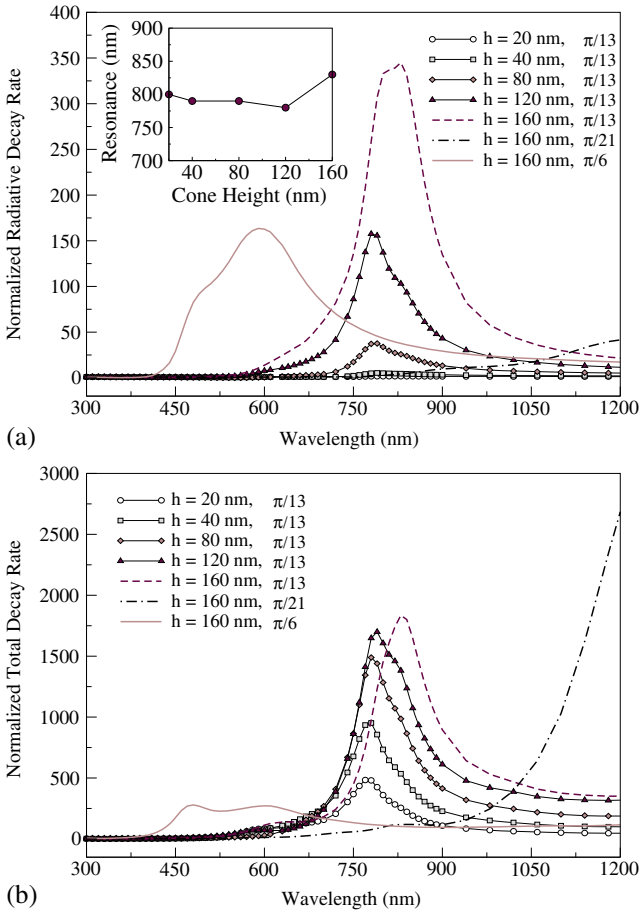

Fig. 5 **a** Normalized radiative decay rates for cones with the same aperture ($\pi/13$ rad) and different heights h (20, 40, 80, 120, and 160 nm), as well as for two cones with h=160 nm and different apertures ($\pi/21$ rad, and $\pi/6$ rad). The distance of the emitter from the tip is fixed to 10 nm. The interdipole distances used in the DDA simulations change according to the cone height: $d_{\text{int}} = 1/16$ nm for $h = 20$ nm, $d_{\text{int}} = 1/8$ nm for $h = 40$ nm, $d_{\text{int}} = 1/4$ nm for $h = 80$ nm, and $d_{\text{int}} = 1/2$ nm for $h = 120$ nm and $h = 160$ nm. The decay rates (Γ) are normalized to the free-space total decay rate of the dipole (Γ_0), and the resonance wavelength for the $\pi/13$ aperture is reported in the inset as a function of h. **b** Normalized total decay rates for the systems in **a**

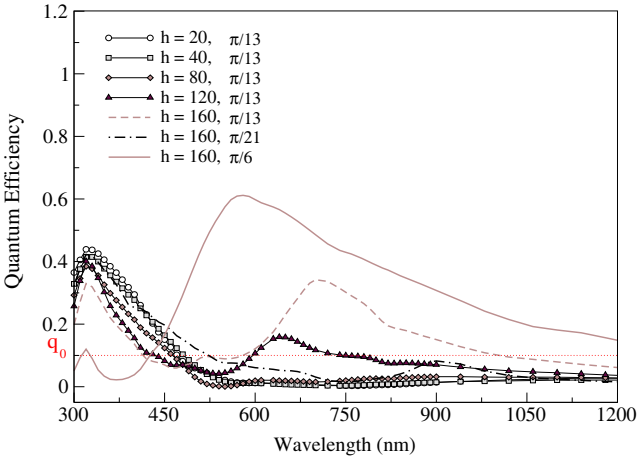

Fig. 6 Quantum efficiencies for the systems in Fig. 5

In Fig. 5a, it results evident how the major role in shifting the resonance frequency must be ascribed to the aperture: cones with the same aperture have the resonance in the same spectral range (around 770 nm) with comparable intensities, while cones with the same height but different tip angles have a completely different resonant behavior. By observing Fig. 5a, we note that the 160-nm high cones with apertures $\pi/21$ and $\pi/6$ have the resonance in similar spectral positions as the previous 20-nm high cone with corresponding aperture. Concerning the peak positions, the total decay rates reported in Fig. 5b behave like the radiative ones: the aperture seems to be the central parameter in shifting the resonance in the spectral range. Moreover, as for $h = 20$ nm (Fig. 3b), the intensity decreases with increasing tip angle.

In Fig. 6, the quantum efficiencies q, defined as the ratio between the radiative and the total decay rate ($q = \Gamma_R/\Gamma$) of the seven different systems analyzed in Fig. 5, are visualized. Here, a dipole with a low intrinsic quantum yield $q_0 = 0.1$ has been considered in the general formula for the quantum efficiency. The relevant wavelength region to consider is $\lambda_{\text{exc}} > 450$ nm where lifetime is strongly modified by the nanocones (see Fig. 5b). For $\lambda_{\text{exc}} < 450$ nm, there is no effect on the lifetime (the quantum yield is high only because nanocones absorb weakly). To obtain an optical "gain" in terms of radiated emission or to improve the quantum yield of an emitter, big Ag cones must be considered (cones with $h = 160$ nm and aperture $\pi/6$). Size is, therefore, the crucial parameter to handle in view of exploiting dipole–nanoantenna interaction for fluorescence enhancement applications.

Conclusion

We have presented a study of the decay rate dynamics for a dipole exciting finite Ag cones with sharp tips, which can be viewed as a *numerical engineering* of the decay rates. We assert the importance of the aperture in shifting the resonances in the desired spectral range and in tuning the enhancements of the radiative and nonradiative decay rates of the dipole. For a given size, an optimal aperture exists for what concerns the radiative efficiency of these structures. Nonradiative decay rates instead increase at decreasing aperture angle. The outcome of the analysis is to achieve, by a numerical point of view, a good control of the lifetime and of the fluorescence quantum yield for a single dipole emitter. The structures can be tailored to achieve high spectral selectivity, by simply handling the geometrical degrees of freedom. By changing the aperture, the dipole resonances can be tuned all over the visible spectrum, while by increasing the size, high quantum efficiencies can be achieved. The results show that metallic nanocones are suitable systems to obtain significant modifications of the spontaneous emission dynamics, towards a numerical engineering of decay rates exploiting surface plasmon resonances and in view of experimental control. The same approach based on the discrete dipole approximation can be applied to nanoantennas of different shapes.

Acknowledgments This work was funded by Fondazione Cariplo under project no. 2010-0523 and by the European Research Council Starting Grant Project DEDOM, grant agreement no. 207441. For computational facilities, S. D. thanks the Italian Institute of Technology with the cluster administrator Dr. Akhilesh Tanwar, and the CINECA Consortium for its technical support (ISCRA Award N. HP10C1ZQTO, 2011).

References

1. Bharadwaj P, Deutsch B, Novotny L (2009) Optical antennas. Adv Opt Photon 1:438
2. Kühn S, Hakanson U, Rogobete L, Sandoghdar V (2006) Enhancement of single-molecule fluorescence using a gold nanoparticle as an optical nanoantenna. Phys Rev Lett 97:017402-1
3. Schuller JA, Barnard ES, Cai WS, Yun YC, White JS, Brongersma ML (2010) Plasmonics for extreme light concentration and manipulation. Nat Mater 9:193
4. Anger P, Bharadwaj P, Novotny L (2006) Enhancement and quenching of single-molecule fluorescence. Phys Rev Lett 96:113002-1
5. D'Agostino S, Pompa PP, Chiuri R, Phaneuf RJ, Britti DG, Rinaldi R, Cingolani R, Della Sala F (2009) Enhanced fluorescence by metal nanospheres on metal substrates. Opt Lett 34:2381
6. Guo SH, Tsai SJ, Kan HC, Tsai DH, Zachariah MR, Phaneuf RJ (2008) The effect of an active substrate on nanoparticle-enhanced fluorescence. Adv Mat 20:1424
7. Mühlschlegel P, Eisler HJ, Martin OJF, Hecht B, Pohl W (2005) Resonant optical antennas. Science 308:1607
8. Taminiau TH, Stefani FD, Segerink FB, van Hulst NF (2008) Optical antennas direct single-molecule emission. Nat Photon 2: 234
9. Chen H, Schatz GC, Ratner MA (2012) Experimental and theoretical studies of plasmon-molecule interactions. Rep Prog Phys 75:096402-1
10. Höppener C, Novotny L (2012) Exploiting the light-metal interaction for biomolecular sensing and imaging. Q Rev Biophys 45: 209
11. Jain PK, Huang X, El-Sayed IH, El-Sayed MA (2007) Review of some interesting surface plasmon resonance-enhanced properties of noble metal nanoparticles and their applications to biosystems. Plasmonics 2:107
12. De Angelis F, Das G, Candeloro P, Patrini M, Galli M, Bek A, Lazzarino M, Maksymov I, Liberale C, Andreani LC, Di Fabrizio E (2010) Nanoscale chemical mapping using three-dimensional adaibatic compression of surface plasmon polaritons. Nat Nanotechnol 5:67–72
13. De Angelis F, Gentile F, Mecarini F, Das G, Moretti M, Candeloro P, Coluccio ML, Cojoc G, Accardo A, Liberale C, Zaccaria RP, Perozziello G, Tirinato L, Toma A, Cuda G, Cingolani R, Di Fabrizio R (2011) Breaking the diffusion limit with super-hydrophobic delivery of molecules to plasmonic nanofocusing SERS structures. Nat Photonics 5:682
14. Berweger S, Atkin JM, Olmon RL, Raschke MB (2012) Light on the tip of a needle: plasmonic nanofocusing for spectroscopy on the nanoscale. J Phys Chem Lett 3:945
15. Maksymov IS, Miroshnichenko AE (2011) Active control over nanofocusing with nanorod plasmonic antennas. Opt Express 19:5888
16. Maksymov IS, Davoyan AR, Kivshar YS (2011) Enhanced emission and light control with tapered plasmonic nanoantennas. Appl Phys Lett 99:083304
17. Stokes N, Cortie MB, Davis TJ, McDonagh AM (2012) Plasmon resonances in V-shaped gold nanostructures. Plasmonics 7:235
18. Stockman MI (2004) Nanofocusing of optical energy in tapered plasmonic waveguides. Phys Rev Lett 93:137404-1
19. Sederberg S, Elezzabi AY (2011) Nanoscale plasmonic contour bowtie antenna operating in the mid-infrared. Opt Express 19: 15532
20. Rao S, Huttunen MJ, Kontio JM, Makitalo J, Viljanen MR, Simonen J, Kauranen M, Petrov D (2010) Tip-enhanced Raman scattering from bridged nanocones. Opt Express 18:23790
21. Gartia MR, Hsiao A, Sivaguru M, Chen Y, Liu GL (2011) Enhanced 3D fluorescence live cell imaging on nanoplasmonic substrate. Nanotechnology 22:365203
22. Hillenbrand R, Taubner T, Keilmann F (2002) Phonon-enhanced light-matter interaction at the nanometre scale. Nature 418:159
23. Fillard JP (1996) Near field optics and nanoscopy. World Scientific Publishing Co Pte Ltd, Singapore
24. Nilius N, Ernst N, Freund HJ (2002) Tip influence on plasmon excitations in single gold particles in an STM. Phys Rev B 65: 115421
25. Neacsu CC, Dreyer J, Behr N, Raschke MB (2006) Scanning-probe raman spectroscopy with single-molecule sensitivity. Phys Rev B 73:193406
26. Osawa M (2001) Surface enhanced infrared absorption: topics in applied physics, vol 81. Springer, New York, p 163
27. Canfield BK, Husu H, Laukkanen J, Bai B, Kuittinen M, Turunen J, Kauranen M (2007) Local field asymmetry drives second-harmonic generation in noncentrosym metric nanodimers. Nano Lett 7:1251
28. Jain PK, Huang X, El-Sayed IH, El-Sayed MA (2008) Noble metals on the nanoscale: optical and photothermal properties and

some applications in imaging, sensing, biology, and medicine. Acc Chem Res 41:1578
29. Ropers C, Neacsu CC, Elsaesser T, Albrecht M, Raschke MB, Lienau C (2007) Grating-coupling of surface plasmons onto metallic tips: a nanoconfined light source. Nano Lett 7:2784
30. De Angelis F, Patrini M, Das G, Maksymov I, Galli M, Businaro L, Andreani LC, Di Fabrizio E (2008) A hybrid plasmonic-photonic nanodevice for label-free detection of a few molecules. Nano Lett 8:2321
31. Hsu C, Connor S, Tang M, Cui Y (2008) Wafer-scale silicon nanopillars and nanocones by Langmuir-Blodgett assembly and etching. Appl Phys Lett 93:133109-1
32. Kontio J, Simonen J, Tommila J, Pessa M (2010) Arrays of metallic nanocones fabricated by UV-nanoimprint lithography. Microelectron Eng 87:1711
33. Rahmani A, Chaumet PC, de Fornel F (2001) Environment-induced modification of spontaneous emission: single-molecule near field probe. Phys Rev A 63:023819-1
34. Zhang W, Cuib X, Martin OJF (2009) Local field enhancement of an infinite conical metal tip illuminated by a focused beam. J Raman Spectrosc 40:1338
35. Liaw JW, Chen JH, Chen CS, Kuo MK (2009) Purcell effect of nanoshell dimer on single moleculeś fluorescence. Opt Express 17:13532
36. Ferrie M, Pinna N, Ravaine S, Vallee RA (2011) Wavelength-dependent emission enhancement through the design of active plasmonic nanoantennas. Opt Express 19:17697
37. Teperik TV, Degiron A (2011) Numerical analysis of an optical toroidal antenna coupled to a dipolar emitter. Phys Rev B 83:245408-1
38. Hohenester U, Trügler A (2011) MNPBEM–a Matlab toolbox for the simulation of plasmonic nanoparticles. Comp Phys Comm 183:370
39. Thomas M, Greffet JJ, Carminati R, Arias–Gonzalez JR (2004) Single-molecule spontaneous emission close to adsorbing nanostructures. Appl Phys Lett 85:3863
40. Vandenbem C, Brayer D, Froufe-Perez LS, Carminati R (2010) Controlling the quantum yield of a dipole emitter with coupled plasmonic modes. Phys Rev B 81:085444-1
41. Vandenbem C, Froufe–Perez LS, Carminati R (2009) Fluorescence signal of a single emitter coupled to a nanoparticle through a plasmonic film. J Opt A: Pure Appl Opt 11: 114007-1
42. Froufe–Perez LS, Carminati R (2007) Fluorescence decay rate statistics of a single molecule in a disordered cluster of nanoparticles. Phys Rev A 76:013835-1
43. Issa NA, Guckenberger R (2007) Fluorescence near metal tips: the roles of energy transfer and surface plasmon polaritons. Opt Express 15:12131
44. Rogobete L, Kaminski F, Agio M, Sandoghdar V (2007) Design of plasmonic nanoantennae for enhancing spontaneous emission. Opt Lett 32:1623
45. Mohammadi A, Sandoghdar V, Agio M (2008) Gold nanorods and nanospheroids for enhancing spontaneous emission. New J Phys 10:105015
46. Mohammadi A, Kaminski F, Sandoghdar V, Agio M (2010) Fluorescence enhancement with the optical (Bi-)conical antenna. J Phys Chem C 114:7372
47. Castani E, Boffety M, Carminati R (2010) Fluorescence quenching by a metal nanoparticle in the extreme near-field regime. Opt Lett 35:291
48. Alpeggiani F, D'Agostino S, Andreani LC (2012) Surface plasmons and strong light-matter coupling in metallic nanoshells. Phys Rev B 86:035421-1
49. Draine BT, Flatau PJ (1994) Discrete-dipole approximation for scattering calculations. J Opt Soc Am A 11:1491
50. Amendola V, Bakr OM, Stellacci F (2010) A Study of the surface plasmon resonance of silver nanoparticles by the discrete dipole approximation method: effect of shape, size, structure, and assembly. Plasmonics 5:85
51. Yurkin MA, Hoekstra AG, ADDA. http://code.google.com/p/a-dda/
52. Novotny L (1996) Single molecule fluorescence in inhomogeneous environments. Appl Phys Lett 69:3806
53. Palik ED (1985) Handbook of optical constants of solids. Academic, New York
54. Khlebtsov NG (2008) Optics and biophotonics of nanoparticles with a plasmon resonance. Quantum Electron 38:504